The Three-dimensional Structure of the Na,K-ATPase from Electron Microscopy

Manijeh Mohraz, Marcia V. Simpson, and P. R. Smith

Department of Cell Biology, New York University School of Medicine, New York 10016

Abstract. The structure of Na,K-ATPase has been studied by electron microscopy and image reconstruction. A three-dimensional structure of this enzyme has been obtained to an overall resolution of 2.5 nm using data from specimens of negatively stained dimer sheets tilted through a range of angles ±60°.

The reconstruction shows a complex mass distribution consisting of ribbons of paired molecules extending ~6.0 nm from the cytoplasmic side of the membrane. The molecular envelope consists of a massive "body" with "lobe" and "arm" structures projecting from it. The body has a columnar shape and is tilted with respect to the plane of the membrane. The region of interaction responsible for dimer formation is located between two bodies and is clearly visible in the reconstruction. It has been identified as a segment in the amino-terminal portion of the α subunit. The arms that interconnect the ribbons are located close to the membrane and are most probably formed by the β subunits.

Na,K-ATPase constitutes the ion pump that couples the hydrolysis of ATP to the transmembrane transport of sodium and potassium ions. It is primarily responsible for the establishment and maintenance of the gradients of Na^+ and K^+ across the plasma membrane of eukaryotic cells. The transmembrane potential produced by this process is used by the cell to power other transport processes. The enzyme is built from two polypeptide chains (7, 14, 16, 20), of which α (M_r 110,000) is the catalytic subunit and β (M_r 50,000–60,000) is a glycoprotein whose function has yet to be determined.

The availability of purified specimens of Na,K-ATPase has allowed extensive studies of its various properties (for reviews see references 5, 10, 17, 32). The recent progress in structural studies of the enzyme has been particularly impressive. The amino acid sequence of α (18, 34) and β (19, 29, 33) have been determined from various tissues. Furthermore, the discovery of crystallization schemes that produced regular arrays of the enzyme in membrane fragments (35) initiated structural studies by electron microscopy and image processing. Structural analyses of the enzyme in projection have been reported (11, 23, 42) as well as preliminary data on its three-dimensional structure (13, 27, 31). In this laboratory we have tentatively mapped the domains in the projection image of the enzyme that correspond to its two subunits (23, 25), and have found reliable crystallization methods to produce regular sheets of the enzyme in a p2 lattice (26).

In this paper we present a three-dimensional structural study of Na,K-ATPase to an overall resolution of 2.5 nm. The reconstruction shows the structure of the enzyme on the cytoplasmic side of the membrane, and reveals that it consists of tilted columns of mass interconnected by a complex set of bridges. These bridges can be identified with the bonds responsible for dimer formation and the subsequent ribbon–ribbon interaction. A segment of the amino-terminal of the α subunit can be located within the structure and a tentative identification for the β subunit can be made. We expect the structure presented here to provide a valuable tool for the integration of emerging structural information concerning this enzyme.

Materials and Methods

Materials

Highly pure bee venom phospholipase A_2 was a gift from Dr. Peter Elsbach, Department of Medicine. Dog kidneys were obtained from the Department of Experimental Surgery of the New York University Medical Center. All chemicals were of the highest available purity.

Purification and Crystallization

Na,K-ATPase was purified in its membrane-associated form from dog kidneys as described previously (26). The enzyme was resuspended at a protein concentration of 1.5–2.0 mg/ml in Imidazole/EDTA buffer (25 mM Imidazole, 1 mM EDTA, 10% sucrose, 0.01% NaN_3, pH 7.5). The suspensions were frozen in liquid N_2 and stored at −25°C. The procedures for the incubation of Na,K-ATPase with phospholipase A_2, and generation of dimeric sheets, have been described in detail elsewhere (26). For the studies reported here, the purified ATPase was suspended at a concentration of 5.0 μg/ml in 10 mM Tris–HCl buffer, pH 7.5, containing 1.0–2.0 U/ml of phospholipase A_2 (1 U hydrolizes 1.0 μmol of L-α-phosphatidylcholine to L-α-lysophosphatidylcholine per minute at pH 8.9 at 25°C). The suspension was dialyzed at 4°C against 10 mM Tris–HCl, 5 mM $CaCl_2$, 5 mM $MgCl_2$, 1 mM $NaVO_3$, pH 7.5. Bacterial growth was inhibited by the addition of 0.005% NaN_3. After the crystallization process was completed (18 to 24 h), the contents of the dialysis bags were pelleted, and the pellets were resuspended in the dialysis buffer at a concentration of 0.2–0.5 mg/ml and stored at 4°C.

Electron Microscopy

Specimens were adsorbed to freshly glow-discharged, carbon-coated grids and were stained with 1% aqueous uranyl acetate. They were visualized in a JEOL 1200EX electron microscope operating at 80 kV. Micrographs were recorded on 4489 Kodak film at a nominal magnification of 75,000. Microscope magnification was calibrated internally using the 4.1-nm striations of T-even phage tails (28).

Tilt series were recorded from selected sheets of the enzyme which appeared most regular. The specimens were tilted through both positive and negative angles and micrographs were recorded at 60, 55, 50, 45, and 30°. Zero tilt images were recorded at the beginning, in the middle, and at the end of the series. Side views were obtained when the sheets appeared to curl up at their edges. Very rarely these were located on sheets which were part of tilt series: oblique views of these sheets showed that the molecules being viewed side-on were not regularly ordered.

Every effort was made to record images as rapidly as possible to minimize the effects of beam damage by following the conventional low-dose procedure of Williams and Fisher (40). The use of this procedure has been estimated to deposit ~5,000–10,000 electrons per square nanometer on the specimen for each image recorded. We were unable to use very low dose techniques in this study. The small size of the crystalline patches, and still smaller size of areas which could be used for computer analysis, required the use of higher doses to provide good contrast for direct visualization of the sheets. Because of these limitations we also decided to collect tilt series from well-ordered sheets rather than to record random tilt images, as had been done in earlier studies of larger and better-ordered crystalline sheets such as actin (37).

Image Processing

Image processing was performed essentially as described by Aebi et al. (1). Selected tilt series were scanned on an Optronics Photoscan (P1000) drum scanner on a 25-μm raster, corresponding to a sampling distance of ~0.4 nm on the specimen. All micrographs were scanned parallel to the *b* axis of the crystalline array. In each series identical areas of at least 100 unit cells were averaged in the filtration process to yield single unit cells for each set of tilt parameters.

Synthesis of the images of the tilted molecule into a three-dimensional reconstruction was performed according to the basic method of Fuller et al. (9), essentially as described previously by Smith et al. (37). Image alignment was done by cross-correlation, initially against a synthetic reference image generated from previously aligned images, and then in a final step, against projections extracted from a preliminary reconstruction.

The irregularly sampled data for the three-dimensional Fourier transform was averaged and interpolated to equally spaced samples using a sinc-function algorithm (36) which also extrapolates into the empty cone of views in a manner consistent with the spatial boundedness of the specimen. It was found that the addition to or deletion from the data set of single tilt images did not appreciably alter the final reconstruction because of the averaging performed during reconstruction generation. Data from the side views was added into the reconstructed transform on the Z^* axis only.

Once the final averaged 3-D transform was obtained, an "*R*-factor" was calculated as:

$$R = \sum_i |A_i - D_i| / \sum_i (|A_i| + |D_i|)$$

where the sum runs over all Fourier terms in all tilts, the *A*'s are the terms extracted from the 3-D transform and the *D*'s are the corresponding datum values from the filtered projected views. This *R*-factor runs from 100% if *A* and *D* are anticorrelated to 0% if they are identical.

After reverse three-dimensional Fourier transformation, the reconstruction was computed on planes parallel to the membrane, separated by a distance of 0.577 nm, and a balsa wood model was constructed from it.

Results

Dimeric Sheets of Na,K-ATPase

Dimer sheets of the enzyme (Fig. 1) were induced using phospholipase A_2 as described in Materials and Methods. The lattice parameters of these specimens were as follows: $a = 14.35$ nm, $b = 4.9$ nm, and $\gamma = 98°$. These values are compared in Table I with those published by other workers for their dimer sheets.

The absolute hand of the sheets was chosen as follows. All images selected, and indeed nearly all phospholipase A_2–induced dimer sheets, showed the same handedness for the arrays indicating that they had the same side of the sheet in contact with the support film. Our studies of freeze-dried and metal shadowed monomeric crystals of the enzyme had revealed that the two surfaces of the sheets had different morphologies. The surface that was predominantly exposed to

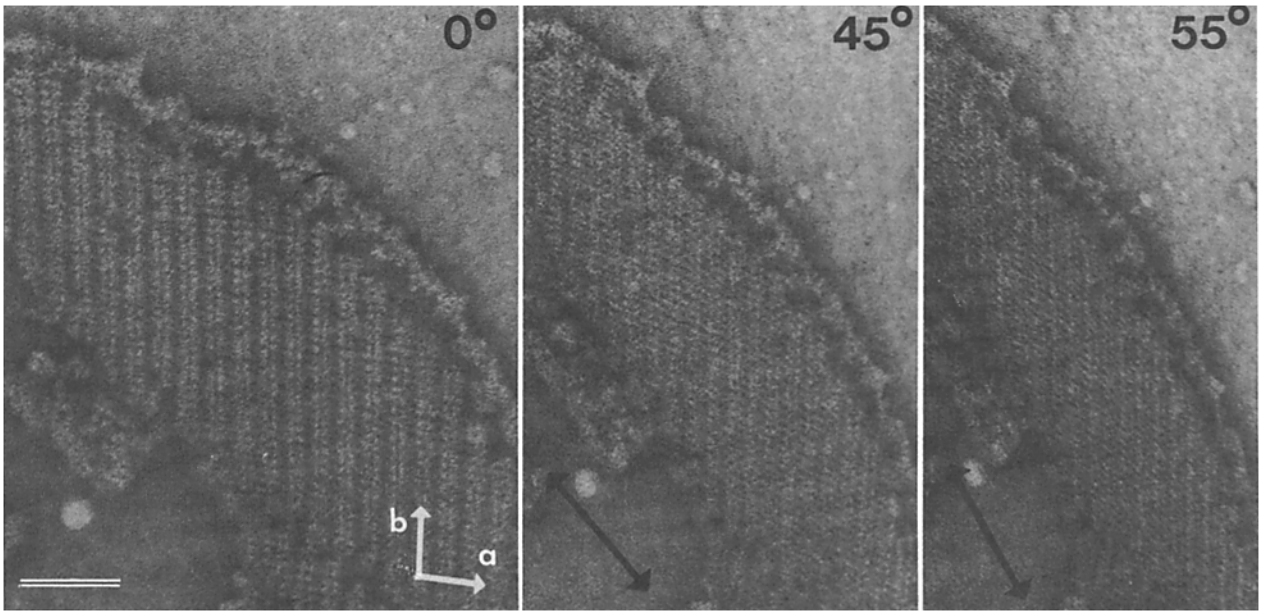

Figure 1. An example of a typical tilt series of one of the phospholipase A_2–induced dimer sheets. The diagonal double-headed arrows in the 45° and 55° tilt images show the direction of the tilt axis with respect to the specimen. The white arrows indicate the directions of the *a* and *b* lattice vectors. Bar, 100 nm.

Table I. Lattice Constants of the Dimeric Crystalline Sheets of Na,K-ATPase

Reference	Study	Hand	Lattice constants			
			a	*b*	γ	*a/b*
			nm	*nm*		
11*	2-D	R	13.4	4.4	98°	3.0
23‡	2-D	L	14.8	5.5	94°	2.7
42	2-D	L	12.5	5.5	110°–126°	2.3
26‡	2-D	R	14.4	4.9	98°	2.9
12	2-D	L	11.3–12.0	4.5–4.6	97°–107°	2.5–2.7
13	3-D	R	12.6	7.6	96.5°	1.7
31	3-D	R	11.8	6.6	108°	1.8

The values for the published lattice constants of dimeric ATPase sheets are presented by reference. The designation "2-D" or "3-D" indicates whether the type of study performed was a two-dimensional filtration or a three-dimensional reconstruction. The choice of hand made for the presentation of micrographs of dimer sheets has not been consistent in the published work. The hand initially chosen by Hebert et al. (11), indicated by *R*, corresponds to the correct absolute hand of the specimen; *L* indicates the opposite hand. The ratio *a/b* is independent of any differences in the overall magnification used in its determination.

* The lattice parameters have been recalculated so as to conform to the standard convention (12).

‡ In these papers the crystallographic axes were chosen to follow the stained outlines of the protein subunits, following electron microscopical convention. According to this convention the lattice constants of the phospholipase A_2 induced dimer sheets are as follows: a = 15.8 nm, b = 4.9 nm, γ = 64°. For the purposes of comparison with other work in this table, these values have been converted so as to conform to the standard convention (12).

the metal beam was rough and showed considerable relief while the other, which was seen only rarely, appeared smooth (24). Since it has been demonstrated that most of the mass of the enzyme protruding from the membrane is located on the cytoplasmic side (e.g., reference 30), we attribute the rough surface of the sheets to the cytoplasmic side of the plasma membrane. We conclude that the exoplasmic side (the smooth surface) of the sheets is in contact with the grid, and that the images of the sheets are views from within the cell looking at the plasma membrane.

From an inspection of Table I it is clear that the absolute hand of the sheets was not established in previous work. Our determination of the absolute hand conforms to the choice made by Hebert et al. (13) and Mohraz et al. (26).

Recording of Micrographs

Micrographs were recorded from specimens of dimer sheets at positive and negative tilts of 60, 55, 50, 45, and 30°, as described in Materials and Methods. Tilt series (e.g., Fig. 1) were selected for further processing on the basis of uniform staining, appropriate level of focus, location of the tilt axis in the specimen, and satisfactory appearance of the diffraction patterns of all members of the series showing preservation of image resolution to at least 3.0 nm (e.g., Fig. 2). The first and last images recorded in a series were always zero tilts and a series was discarded if these zero tilt images appeared significantly different either visually or by optical diffraction. The extent of specimen degradation could also be assessed from the comparison of these images. It was found that <1.5% of the recoverable dynamic power was lost due to beam damage or other degradative processes during the recording of the tilt series. A power loss this small indicates that the structural alterations induced by the beam are negligible for this specimen in the accessible resolution range.

A total of seven tilt series were selected for further processing and representative images are shown in Fig. 1. Tilts in the range of 0 to +60° were digitized and computer filtered to yield 42 independent projection images of the dimer sheets. The images that were of high visual quality and that had clean uncluttered diffraction patterns also showed a high degree of twofold symmetry. All the arrays used in the reconstruction had power losses of <5% on symmetrization, and for most the power loss was <1%.

Initial image alignment and scaling was performed using the standard schemes developed by Fuller et al. (9). The alignment was refined by cross-correlating the data images with central sections extracted from a preliminary 3-D transform (8, 37). Input data to all lattice lines were band-limited to a resolution of ~2.0 nm in the Z^* direction for the computation of the final reconstruction. This was generated from the aligned image data using the sinc-function interpolation method (36).

Side View Data from the Sheets

Side views of the sheets were observed at the curled edges of membrane patches. Characteristic images show rows of

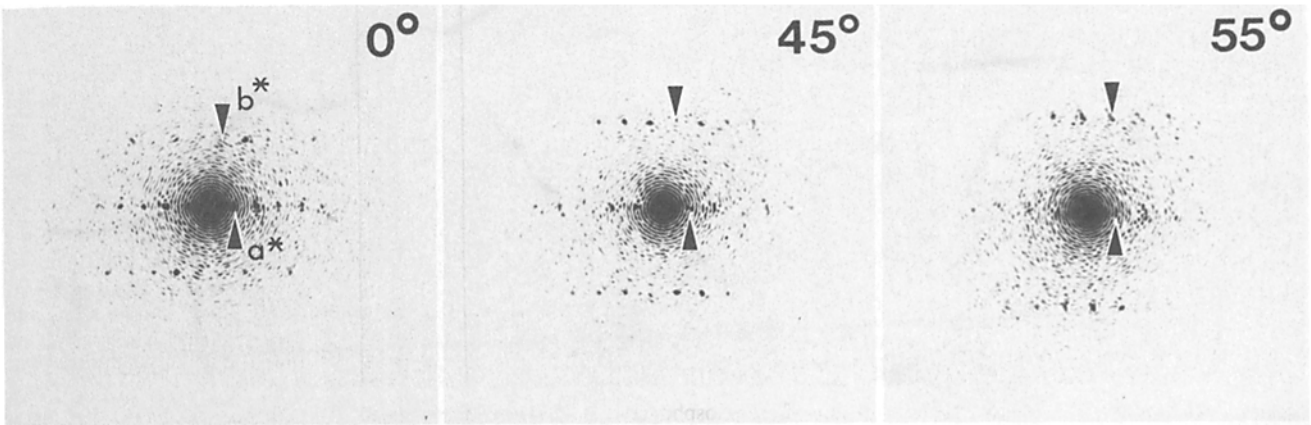

Figure 2. Optical diffraction patterns from the elements of the tilt series shown in Fig. 1. The arrowheads indicate the locations of the first order spots in the a^* and b^* reciprocal lattice directions for each tilt.

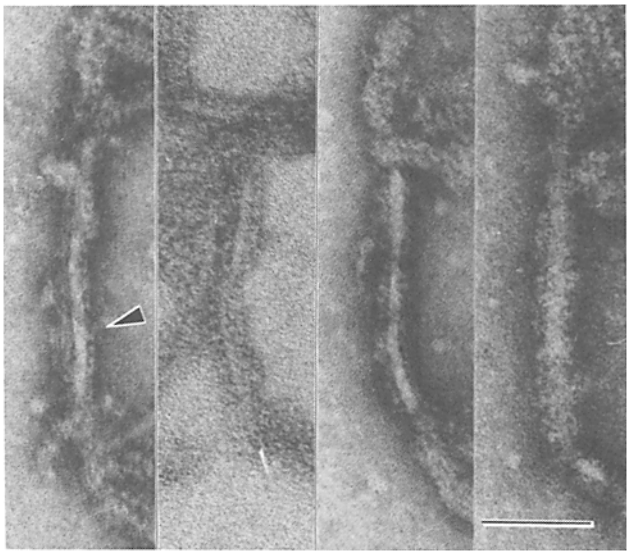

Figure 3. Representative side views of the dimer sheets showing edge-on views of the membrane fragments with ATPase molecules protruding from them. One side of one of these fragments (*arrowhead*) provided a projection view of the cytoplasmic portion of the ATPase, which was used in the reconstruction. Bar, 50 nm.

"balls on sticks" attached to the two sides of the membrane, with the balls located ~6.0 nm from the membrane (Fig. 3), and stain-excluding and stain-penetrated regions opposite one another. These structures were found to be spaced between 4.5–9.0 nm apart in various specimens. In rare views where tilting revealed a glimpse of a fragment that was edge-on in vertical projection, the particles on its surface were seen to be disordered.

Since the crystallinity of the specimens visualized in edge views was not assured, the information provided by these images was limited to the mass distribution perpendicular to the plane of the membrane since these data are unaffected by the orientation of the molecules. An image was selected with an interparticle spacing of 5.5 nm, which is similar to the spacing of the unit cells in the sheet in the *b* lattice direction. Three repeats were averaged together and the resulting image was compared to the side view of the enzyme obtained from the reconstruction. An orientation of the side view with respect to the reconstruction was then selected, and the Z^* axis information from the side view was transferred to the reconstructed transform.

Consistency of the Data Set

The consistency of the data set was evaluated by inspecting its continuity over the lattice lines after projection image alignment and scaling, as described in Materials and Methods. As expected, the continuity of the estimates after final alignment was best for the strong orders in the image transforms. However, satisfactory lattice line data distributions could be found for nearly all lines. Representative data for three lattice lines are shown in Fig. 4 where phases and amplitudes are plotted for the input datum points on the lattice lines. The interpolated values were obtained from the input data as described previously (36). These values generally followed the path one would select by eye.

In addition, projection images generated from the reconstructed transforms were compared with the filtered images of the tilted specimens used to form the data set. Good agreement was obtained between the micrograph data and the extracted projection images in nearly all cases (data not shown). Finally, an R-factor evaluating the agreement between the input filtered image data and the three-dimensional transform obtained from it was computed (see Materials and Methods) to be 33%, which is a satisfactory value. Taken together these results confirmed that the projections formed a consistent set and that the data had been synthesized correctly in the final three-dimensional transform.

The Three-dimensional Reconstruction

The reconstructed three-dimensional Fourier transform was filled with significant information to five orders in the a^* direction and two orders in b^*. Contributions to the transform were truncated to ~2.0 nm in the Z^* direction. The micrograph data provided good coverage of three-dimensional Fourier space. Fig. 5 shows the distribution of data in Fourier space with arcs drawn to show the relationship between the recorded lattice line data and its resolution. An arc at the 3.0 nm resolution level encloses ~60% of the datum points on the lattice lines, and the arc at the 2.5-nm resolution level encloses ~72% of the datum points on the lattice lines, with the remaining 28% carrying higher resolution information. 2.5 nm is therefore a representative resolution level for the reconstruction as a whole. The interpolation

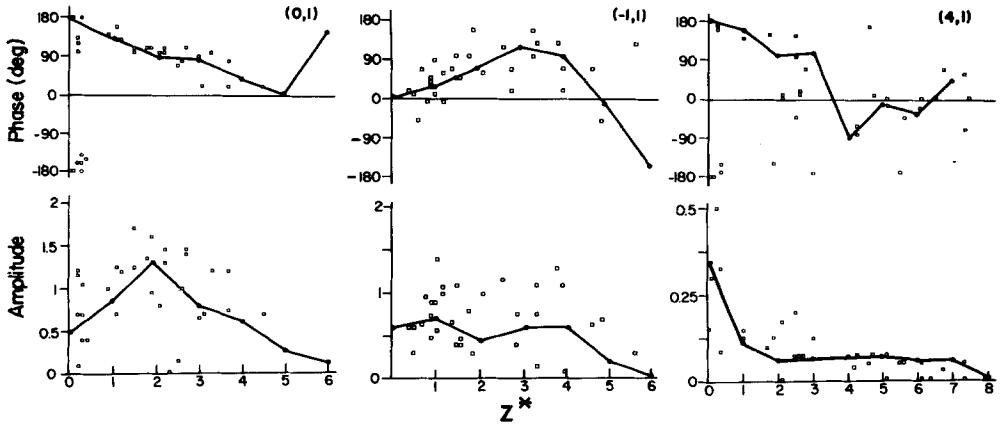

Figure 4. Amplitude and phase plots for three lattice lines in the reconstructed transform. Amplitudes are shown in arbitrary units, phases are in degrees. The unit in the Z^* direction is 1/(15 nm), which is the sampling distance used in this direction in the computation of the reconstruction. Individual datum points are indicated by open squares, the interpolated values at the sample points are indicated by solid squares. The lines that connect these points are intended to guide the eye.

program extrapolated values into the entire transform in the Z^* direction to ensure that the reconstruction was spacially bounded to 15.0 nm (36). Reverse Fourier transformation yielded a reconstruction that was represented on a series of 26 slices parallel to the plane of the membrane and separated by 0.577 nm. The depth of the reconstruction (15.0 nm) was therefore sufficient to accommodate the full expected thickness of the sheet (11.5 nm), leaving room for additional structures or noise contributions that would otherwise contaminate the reconstruction via aliasing: however, no such structures were found.

The reconstruction showed high contrast structural features in only a limited volume. This was a region ~6.0 nm in depth, abutting one side of the membrane. Since the majority of the molecular mass is located on the cytoplasmic side of the membrane (30), and little structure can be visualized on the exoplasmic side by freeze-drying (24), we attribute the structure we observe to the cytoplasmic side of the membrane only. Fig. 6 therefore shows a balsa wood model of the reconstruction of the cytoplasmic component of the dimer sheet. Fig. 6 *a* is a view from the inside of the cell perpendicular to the membrane, and Fig. 6 *b* is a side view of the model. The unit cell volume was computed for the reconstruction at a number of contour levels. The chosen contour level, which was used to build the model in Fig. 6, contains a volume for the unit cell of 170 cubic nm and an estimated protein mass of 144,000 daltons, which is a reasonable estimate for the mass of a dimer of the enzyme protruding from the cytoplasmic side of the membrane.

The reconstruction shows a complex mass distribution consisting of ribbons of paired molecules attached to the membrane and sets of bridges interconnecting them. The massive parts in the molecules are tilted such that their upper levels are displaced with respect to the region adjacent to the membrane (see Figs. 6 *b* and 7). In the neighborhood of the membrane, bridges are seen to run parallel to the *a* lattice vector connecting the bases of the paired stain-excluding regions in each ribbon and continuing to connect adjacent ribbons. Bridges are formed ~3.0 nm from the membrane that connect the molecules in the direction of the *b* lattice vector, which is parallel to the axis of the ribbon. At the upper levels in the reconstruction, linkages join the tops of the tilted molecules, bridging the narrow stain-filled trough at the center of the ribbon. A prominent feature of the reconstruction is the extended arms at the upper levels that nearly join the molecules in a diagonal fashion over the stain trough which separates the ribbons. These are offset with respect to the bridges adjacent to the membrane so that the two are superimposed when the sheet is viewed at 30° tilt.

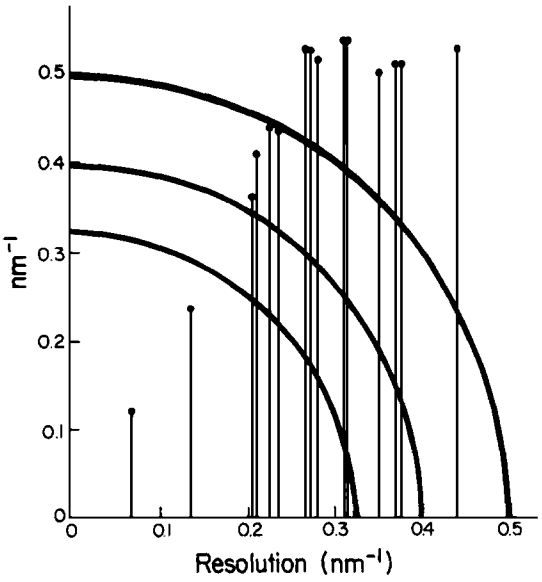

Figure 5. The resolution distribution of the data included in the reconstruction. The inner circle is drawn at a resolution of 3.0 nm and encloses 60% of the datum points on the lattice lines, the intermediate circle is at 2.5 nm and encloses 72% of the datum points, and the outer circle is at 2.0 nm. Most lattice lines contribute some data at a resolution better than 2.0 nm. Given the distribution of the datum points on the lattice lines, 2.5 nm is a representative overall resolution for this reconstruction.

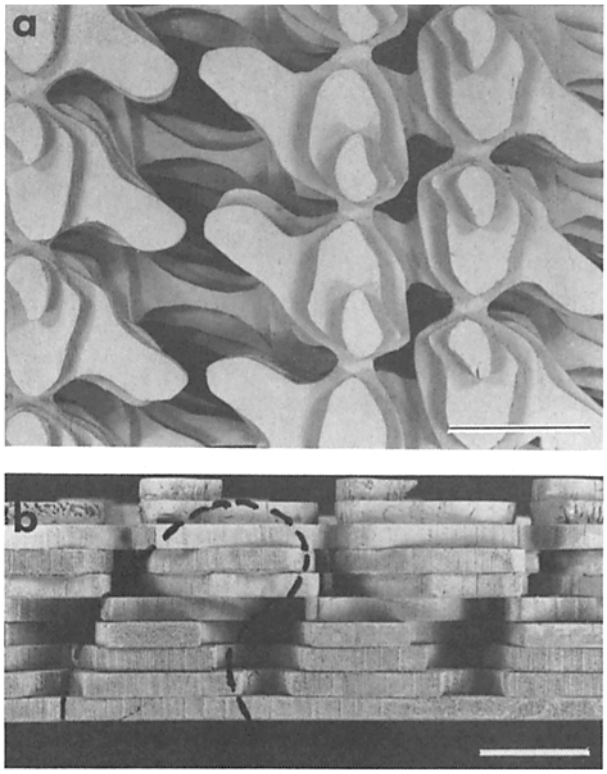

Figure 6. (*a*) Balsa wood model of the reconstruction of Na,K-ATPase viewed from within the cell showing the cytoplasmic component of the dimer sheet. The plasma membrane is located behind the reconstruction. A key to the various structural features is provided by Fig. 7. (*b*) The model viewed parallel to the plane of the membrane. It represents a side view of the reconstruction at the level corresponding to the left hand edge of Fig. 6 *a*. The dotted line demarks one of the tilted ATPase molecules. The black band at the bottom of the figure is the location of the plasma membrane. Bars: (*a*) 5.0 nm; (*b*) 2.5 nm.

Discussion

Our study of the structure of Na,K-ATPase was performed on seven tilt series collected from crystalline sheets induced by phospholipase A_2, VO_3^-, and Mg^{2+} (26). This method of crystallization led to the exclusive formation of extensive di-

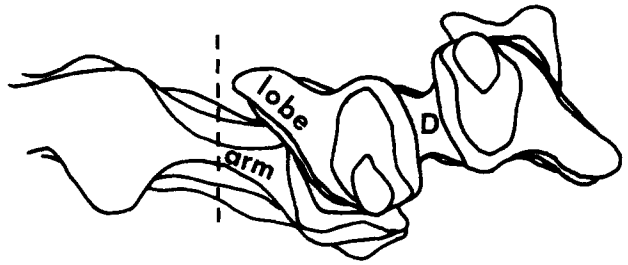

Figure 7. Isodensity contour map, viewed perpendicular to the membrane, as in Fig. 6 *a*. For simplicity only the middle molecule shows the whole volume of the reconstruction, with partial views being shown of the adjacent molecules to emphasize the location of the bridges within the reconstructed volume. The various structural features of the ATPase molecule are labeled. The "lobe" and the "arm" project from the tilted column of mass we have termed the "body." The structure to the right of the dotted line is the dimer. The linkage "*D*" is attributed to an α–α interaction. The inter-ribbon bridge is formed by the arms and is tentatively identified as a β–β interaction.

meric arrays with stable lattice parameters. In the first step of the assembly pathway, pairs of enzyme molecules associated to form long ribbons. These subsequently aggregated laterally to form two-dimensional arrays (26), a mechanism shared with the Ca-ATPase (e.g., reference 4). The spacing of the units along the axis of the ribbons (*b* lattice direction) tended to be constant but the other lattice parameters were subject to small variations that were probably a consequence of weaker interactions between the ribbons.

Our first step in the construction of the model of the enzyme was to inspect the three-dimensional reconstruction without side view data included. All the major features of the molecule, which are discussed in detail below, could be identified in this reconstruction which showed strong structure in only a 6.0-nm deep region of the full 15.0-nm thickness of the reconstruction volume. Outside this 6.0-nm region the mass distribution was of low contrast and disorganized.

To define fully the three-dimensional transform and complete the reconstruction, projection information from the side of the structure must be included in the database. This information was obtained from images such as those in Fig. 3 where molecules of ATPase could be seen protruding from the membrane. These structures often appear quite symmetric in the amount of stain they exclude on the two "sides" of the membrane, which is inconsistent with the known asymmetry in the mass distribution of the molecule (30). Recently, Zampighi et al. (43) have asserted that these images actually show narrow diameter cylinders where the cytoplasmic parts of the molecule protrude from the exposed surface and the transmembrane and exoplasmic parts of the molecule lie buried within. According to their model, side views provide a projection view of the cytoplasmic portion of the ATPase molecules parallel to the membrane.

We chose a side view region where the molecular packing closely approximated the crystal packing along the *b* axis in the sheets. There was close similarity between the side view obtained from the micrograph data and the side view extracted from the three-dimensional reconstruction, and indeed the orientation we had selected gave the best fit between the micrograph and the reconstruction data. This result supported our choice and provided a rationale for selecting a scaling factor for the side view data relative to the incomplete reconstruction (37). The addition of the side view modulated the density values perpendicular to the membrane surface and improved the contrast of the structures that had been visualized, it did not add new features or alter the interpretations already given to them.

The limitation of recoverable information to one side of the membrane has been a common finding in three-dimensional studies of negatively stained specimens of membrane proteins, for example in the bladder membrane (3, 22) and more recently in the reconstruction of the Ca-ATPase (38). In the case of the Na,K-ATPase an explanation may be found in results from freeze-dried and shadowed specimens of ATPase sheets (24) where the exoplasmic surface of the membrane, on the rare occasions it was exposed, was found to show little structure. It is possible that the extended sugar chains attached to the β subunit may collapse during specimen preparation forming a poorly organized meshwork that masks the regular structure of the exoplasmic protein component of the sheet.

The reconstruction we obtain has a number of interesting structural components. The molecule has a massive "body" which is tilted with respect to the plane of the membrane (Fig. 6 *b*). A "lobe" extends from the body in the parts of the molecule furthest from the membrane, and an "arm" projects from it in the region adjacent to the membrane (see Fig. 7). The structural features correspond to those seen previously in the projection images of the molecule (23, 26); however, in the projection images the arm and the lobe appeared superimposed and the structure observed was termed the "hook."

The most prominent feature of the sheet is the dimer ribbon. Within the ribbon, connections are made between each ATPase molecule and its nearest neighbors. Sheet assembly occurs via a series of steps consisting of dimer formation, ribbon assembly, and finally the lateral association of the ribbons to form the sheet. Therefore, the first linkage to form interconnects two ATPase molecules to form the dimer. This linkage can be seen readily in the contour map shown in Fig. 7 and is labeled *D*. It is located at a distance of ~3.5 nm above the membrane, has a thickness of ~1.2 nm and runs nearly perpendicular to the axis of the ribbon. It connects the domains we had previously identified as α subunits, based on the comparison of the projection images of the intact and the trypsin-digested enzyme (23). This trypsin digestion scheme specifically removes a fragment of ~23,000 D from the amino terminal of the α subunit. Since we have never succeeded in forming dimeric arrays in the digested preparations of the enzyme by the phospholipase treatment, we conclude that the interaction responsible for dimer formation is between segments within the digested fragment of the amino termini of the α subunits. This part of the α subunit (linkage *D*) can now be localized in the structure of the ATPase that protrudes from the cytoplasmic side of the membrane. A second, less substantial linkage interconnects molecules parallel to the axis of the ribbon at a level of ~3.0 nm above the membrane. Finally, adjacent to the membrane the ATPase molecules are seen to connect via their bases along a line parallel to the inter-ribbon linkages. This link appears substantial, but its location deep within the ribbon may contribute to the relative lack of stain in this region.

The ribbons themselves are interconnected by the arm

structures (see Fig. 7). The arms were tentatively ascribed in the projection images to the β subunit of the ATPase (23). Since the β subunit protrudes only slightly from the cytoplasmic side of the membrane, the finding that these features are located adjacent to the membrane tends to support this identification. The lobe structure extends from the upper part of the ATPase molecule into the groove between the ribbons, nearly parallel to the β–β bridges. This feature, identified as a bridge in a preliminary reconstruction (27), is probably associated with the α subunit, based on its location within the structure relative to the membrane.

Two previous reconstructions of dimer sheets of Na,K-ATPase have been published as brief reports by Hebert et al. (13) and Ovchinnikov et al. (31). Their crystallization scheme (11) generates dimer sheets only very rarely and these sheets have variable lattice constants, in contrast to those formed by the phospholipase induction method that we use. Table I demonstrates striking differences among the lattice parameters published by various workers in the field. While it is clear that some of the discrepancies are due to differences in the overall magnification factors, which do not affect the *a/b* ratio, other values cannot be explained in this manner. In particular the lattice constants of the dimer sheets used for reconstruction by Ovchinnikov et al. (31) and Hebert et al. (13) appear different from those we have studied here and also those published by others. Both groups report reconstructing a Na,K-ATPase molecule that spans the membrane and both reconstructions are ~10.0 nm in depth, in contrast to our result which shows structure on one side of the membrane only. A significant technical problem with the work of Hebert et al. (13) is the fact that the reconstruction is derived from only a single tilt series. For this reason their reconstruction contains little information concerning the distribution of stain-excluding structure perpendicular to the membrane. The structure of Ovchinnikov et al. (31) was obtained from five tilt series. However, it is not possible to make direct comparison of their structure with ours since the crystals they analyzed are very different from our own.

The structure of Na,K-ATPase can be compared with that of the Ca-ATPase studied by Taylor et al. (38). The two enzymes are related in that they are transmembrane ion pumps with catalytic subunits that share sequence homologies (34) and that they crystallize via a nucleation step in which dimeric ribbons are formed. The major structural difference between the two enzymes is that the Na,K-ATPase has an additional subunit (β), which the Ca-ATPase lacks. There are interesting similarities between the reconstructions of the two ATPases. Both show the molecule to have a massive body, which is tilted with respect to the membrane, with a lobe projecting from it. In both, the bridges that are responsible for dimer formation are located between the massive domains; however, the configuration of interactions between adjacent molecules in relation to the lobes is different. The major difference between the two reconstructions is in the manner that the ribbons interact laterally to form extended arrays. The interaction between ribbons is poorly defined in the Ca-ATPase where the connections are apparently made within the lipid bilayer. This is in contrast to the Na,K-ATPase where the arms form a clear bridge directly between the adjacent ribbons (Fig. 7). The lack of this structural feature in the Ca-ATPase provides further support for attributing it to a β–β interaction in Na,K-ATPase.

The structure of Na,K-ATPase shows considerable detail, but it is difficult to associate any of these features with structures involved in specific aspects of the pumping function of the enzyme. An example of a structure with which to compare it is the photosynthetic membrane of the photosynthetic bacterium *Rhodopseudomonas viridis*, which has light harvesting and transmembrane electron transport components (15). In this structure no pore can be visualized at the 2.0–2.5-nm resolution in any component of the membrane (21). Indeed, at the 0.3-nm resolution the reaction center, where the primary charge separation occurs, shows no hint of a channel region (6). Therefore, it would be unlikely that in Na,K-ATPase structural features at the 2.5-nm resolution could be linked to pump function. In fact, the sodium ion is small enough that it could leave the cell through a transmembrane α helix and the potassium ion, which is somewhat larger, could presumably be transported between transmembrane elements. In contrast to these systems, structures such as gap junctions (e.g., references 39, 41) and acetylcholine receptors (e.g., reference 2) whose function is to provide unrestricted flow of ions and small molecules across the membrane readily reveal the presence of pores.

The structure determined here provides a first attempt to define an envelope for the molecule. We expect this envelope to be a stable and reliable model for the enzyme in the 2.5-nm resolution range. The structure has provided additional support for our previous work, where we had tentatively identified the locations of the α and the β subunits in the projection image of the enzyme molecule. Furthermore, we have been able to localize the amino-terminal portion of the α subunit within the three-dimensional structure. We expect this structure to provide a framework for organizing emerging biochemical and complementary structural information and to allow such new information to be integrated and eventually interpreted in functional terms.

We are particularly grateful to Movien Yee for excellent technical assistance, and to Dr. E. L. Buhle, Jr., for help with image digitization and display. Drs. Takashi Morimoto and Ueli Aebi are thanked for valuable discussions.

The work was supported by grants GM-26723 and GM-35399 from the National Institute for General Medical Sciences, and by Digital Equipment Corporation through the gift of a PDP 11-44 computer (to P. R. Smith) which was used for the majority of the computations.

Received for publication 13 August 1986, and in revised form 4 February 1987.

References

1. Aebi, U., W. E. Fowler, G. Isenberg, T. D. Pollard, and P. R. Smith. 1981. Crystalline actin sheets: their structure and polymorphism. *J. Cell Biol.* 91:340–351.
2. Brisson, A., and P. N. T. Unwin. 1984. Tubular crystals of acetylcholine receptor. *J. Cell Biol.* 99:1202–1211.
3. Brisson, A., and R. H. Wade. 1983. Three-dimensional structure of luminal plasma membrane protein from urinary bladder. *J. Mol. Biol.* 166: 21–36.
4. Buhle, E. L., Jr, B. E. Knox, E. Serpersu, and U. Aebi. 1983. The structure of the Ca^{2+}ATPase as revealed by electron microscopy and image processing of ordered arrays. *J. Ultrastruct. Res.* 85:186–203.
5. Cantley, L. C. 1981. Structure and mechanism of the (Na,K)-ATPase. *Curr. Top. Bioenerg.* 2:201–237.
6. Deisenhofer, J., O. Epp, K. Miki, R. Huber, and H. Michel. 1984. X-ray structure analysis of a membrane protein complex. Electron density map at 3Å resolution and a model of the chromophores of the photosynthetic reaction center from *Rhodopseudomonas viridis*. *J. Mol. Biol.* 180:385–398.
7. Dixon, J. F., and L. E. Hokin. 1974. Studies on the characterization of the sodium-potassium transport adenosine triphosphatase. *Arch. Biochem. Biophys.* 163:749–758.
8. Engel, A., and A. Massalski. 1984. 3D reconstruction from electron micro-

graphs: its potential and practical limitations. *Ultramicroscopy.* 13:71–83.
9. Fuller, S. D., R. A. Capaldi, and R. Henderson. 1979. Structure of cytochrome c oxidase in deoxycholate-derived two-dimensional crystals. *J. Mol. Biol.* 134:305–327.
10. Glynn, I. M. 1985. The Na^+,K^+-transporting adenosine triphosphatase. *In* The Enzymes of Biological Membranes. Vol. 3. Martonosi, A. N., editor. Plenum Publishing Corp., New York and London. 35–114.
11. Hebert, H., P. L. Jorgensen, E. Skriver, and A. B. Maunsbach. 1982. Crystallization patterns of membrane-bound (Na^+,K^+)-ATPase. *Biochim. Biophys. Acta.* 689:571–574.
12. Hebert, H., E. Skriver, R. Hegerl, and A. B. Maunsbach. 1985. Structure of two-dimensional crystals of membrane-bound Na,K-ATPase as analysed by correlation averaging. *J. Ultrastruct. Res.* 92:28–35.
13. Hebert, H., E. Skriver, and A. B. Maunsbach. 1985. Three-dimensional structure of renal Na,K-ATPase determined by electron microscopy of membrane crystals. *FEBS (Fed. Eur. Biochem. Soc.) Lett.* 187:182–186.
14. Hokin, L. E., J. L. Dahl, J. D. Deupree, J. F. Dixon, J. F. Hackney, and J. F. Perdue. 1973. Studies on the characterization of the sodium-potassium transport adenosine triphosphatase. *J. Biol. Chem.* 248:2593–2605.
15. Jacob, J. S., and K. R. Miller. 1983. Structure of a bacterial photosynthetic membrane. Isolation, polypeptide composition, and selective proteolysis. *Arch. Biochem. Biophys.* 223:282–290.
16. Jorgensen, P. L. 1974. Purification and characterisation of (Na^+,K^+)-ATPase. III. Purification from the outer medulla of mammalian kidney after selective removal of membrane components by sodium dodecylsulphate. *Biochim. Biophys. Acta.* 356:36–52.
17. Jorgenson, P. L. 1982. Mechanism of the Na^+,K^+ pump. Protein structure and conformations of the pure (Na^+,K^+)-ATPase from the outer medulla of rabbit kidneys. *Biochim. Biophys. Acta.* 694:27–68.
18. Kawakami, K., S. Noguchi, M. Noda, H. Takahashi, T. Ohta, M. Kawamura, H. Nojima, K. Nagano, T. Hiose, S. Inayama, H. Hayashida, T. Myata, and S. Numa. 1985. Primary structure of the α-subunit of Torpedo californica (Na^+,K^+)ATPase deduced from cDNA sequence. *Nature (Lond.).* 316:733–736.
19. Kawakami, K., H. Nojima, T. Ohta, and K. Nagano. 1986. Molecular Cloning and sequence analysis of human Na,K-ATPase β-subunit. *Nucleic Acids Res.* 14:2833–2844.
20. Kyte, J. 1971. Purification of the sodium- and potassium-dependent adenosine triphosphatase from canine renal medulla. *J. Biol. Chem.* 246:4157–4165.
21. Miller, K. R. 1982. Three-dimensional structure of a photosynthetic membrane. *Nature (Lond.).* 300:53–55.
22. Milligan, R. A., A. Brisson, and P. N. T. Unwin. 1984. Molecular structure determination of crystalline specimens in frozen aqueous solutions. *Ultramicroscopy.* 13:1–9.
23. Mohraz, M., and P. R. Smith. 1984. Structure of (Na^+,K^+)-ATPase as revealed by electron microscopy and image processing. *J. Cell Biol.* 98: 1836–1841.
24. Mohraz, M., C. A. Rinder, M. V. Simpson, and P. R. Smith. 1984. The structure of (Na,K)-ATPase as revealed by electron microscopy. *Ann. N.Y. Acad. Sci.* 435:561–563.
25. Mohraz, M., C. A. Rinder, and P. R. Smith. 1985. Structure of Na,K-ATPase determined by electron microscopy and image processing. *In* The Sodium Pump. Glynn, I. M., and C. Ellory, editors. The Company of Biologists Ltd., Cambridge. 45–49.
26. Mohraz, M., M. Yee, and P. R. Smith. 1985. Novel crystalline sheets of Na,K-ATPase induced by phospholipase A_2. *J. Ultrastruct. Res.* 93: 17–26.
27. Mohraz, M., M. Yee, and P. R. Smith. 1986. Structural studies of Na, K-ATPase. *Ann. N.Y. Acad. Sci.* 438:131–139.
28. Moody, M. F. 1971. Structure of the T2 bacteriophage tail-core, and its relation to the assembly and contraction of the sheath. *In* Proceedings of the First European Biophysics Congress. Broda, E., A. Locker, and H. Springer-Lederer, editors. Verlag der Med. Akad., Wien. 543–546.
29. Noguchi, S., M. Noda, H. Takahashi, K. Kawakami, T. Ohta, K. Nagano, T. Hirose, S. Inayama, M. Kawamura, and S. Numa. 1986. Primary structure of the β subunit of Torpedo californica (Na^+,K^+)-ATPase deduced from the cDNA sequence. *FEBS (Fed. Eur. Biochem. Soc.) Lett.* 196:315–320.
30. Ohta, T., K. Nagano, and M. Yoshida. 1986. The active site structure of Na^+/K^+-transporting ATPase: location of the 5'-(p-fluorosulfonyl)benzoyladenosine binding site and soluble peptides released by trypsin. *Proc. Natl. Acad. Sci. USA.* 83:2071–2075.
31. Ovchinnikov, Y. u. A., V. V. Demin, A. N. Barnakov, A. P. Kuzin, A. V. Lunev, N. N. Modyanov, and K. N. Dzhandzhugazyan. 1985. Three-dimensional structure of ($Na^+ + K^+$)-ATPase revealed by electron microscopy of two-dimensional crystals. *FEBS (Fed. Eur. Biochem. Soc.) Lett.* 190:73–76.
32. Robinson, J. D., and M. S. Flashner. 1979. The (Na^+,K^+)-activated ATPase: enzymatic and transport properties. *Biochim. Biophys. Acta.* 549: 145–176.
33. Shull, G. E., L. K. Lane, and J. B. Lingrel. 1986. Amino-acid sequence of the β subunit of the (Na^+,K^+)ATPase deduced from cDNA. *Nature (Lond.).* 321:429–431.
34. Shull, G. E., A. Schwartz, and J. B. Lingrel. 1985. Amino-acid sequence of the catalytic subunit of ($Na^+ + K^+$)ATPase deduced from a complementary DNA. *Nature (Lond.).* 316:691–695.
35. Skriver, E., A. B. Maunsbach, and P. L. Jorgensen. 1981. Formation of two-dimensional crystals in pure membrane-bound Na^+,K^+-ATPase. *FEBS (Fed. Eur. Biochem. Soc.) Lett.* 131:219–222.
36. Smith, P. R. 1981. The interpolation of Fourier transform data in tilted-view three-dimensional reconstruction. *Ultramicroscopy.* 7:155–160.
37. Smith, P. R., W. E. Fowler, T. D. Pollard, and U. Aebi. 1983. Structure of the actin molecule determined from electron micrographs of crystalline actin sheets with a tentative alignment of the molecule in the actin filament. *J. Mol. Biol.* 167:641–660.
38. Taylor, K. A., L. Dux, and A. Martinosi. 1986. Three-dimensional reconstruction of negatively stained crystals of the Ca^{2+}-ATPase from muscle sarcoplasmic reticulum. *J. Mol. Biol.* 187:417–427.
39. Unwin, P. N. T., and P. D. Ennis. 1984. Two configurations of a channel-forming membrane protein. *Nature (Lond.).* 307:609–613.
40. Williams, R. C., and H. W. Fisher. 1970. Electron microscopy of TMV under conditions of minimal beam exposure. *J. Mol. Biol.* 52:121–123.
41. Zampighi, G., J. M. Corless, and J. D. Robertson. 1980. On gap junction structure. *J. Cell Biol.* 86:190–198.
42. Zampighi, G., J. Kyte, and W. Freytag. 1984. Structural organization of ($Na^+ + K^+$)-ATPase in purified membranes. *J. Cell Biol.* 98:1851–1864.
43. Zampighi, G., S. A. Simon, J. Kyte, and M. Kreman. 1986. One-dimensional crystals of ($Na^+ + K^+$)-ATPase dimers. *Biochim. Biophys. Acta.* 854:45–57.